Thermal Hall effect in noncollinear coplanar insulating antiferromagnets

Alexander Mook,[1] Jürgen Henk,[1] and Ingrid Mertig[1,2]
[1]*Institut für Physik, Martin-Luther-Universität Halle-Wittenberg, D-06099 Halle (Saale), Germany*
[2]*Max-Planck-Institut für Mikrostrukturphysik, D-06120 Halle (Saale), Germany*

(Received 2 November 2018; published 22 January 2019)

We establish theoretically a thermal Hall effect of collective magnetic excitations in noncollinear but coplanar antiferromagnets. In agreement with superordinate symmetry arguments for linear transport tensors, our findings demonstrate that neither a ferromagnetic moment, nor a magnetic field, nor a scalar spin chirality are indispensable for a magnon thermal Hall effect. Similar to the electronic anomalous Hall effect, the two necessary requirements are broken effective time-reversal symmetry and a magnetic point group compatible with ferromagnetism. As an example, we construct a minimal model for an antiferromagnet on the kagome lattice with the coplanar negative vector chiral order. In the presence of in-plane Dzyaloshinskii-Moriya interactions, the coplanar order stays intact but both magnon band gaps and a nonzero Berry curvature develop. This coplanar magnet realizes an antiferromagnetic magnon Chern insulator with a nonzero thermal Hall effect. We propose cadmium kapellasite $CdCu_3(OH)_6(NO_3)_2 \cdot H_2O$ as an approximate material realization.

DOI: 10.1103/PhysRevB.99.014427

I. INTRODUCTION

Antiferromagnets are at the very heart of modern solid state research because they are expected to replace ferromagnetic components in next-generation spintronics devices. Several recent review papers are testament to the broad interest [1–9], originating from the key virtues of antiferromagnets with respect to applications: robustness against magnetic fields, absence of stray fields, and ultrafast dynamics [1]. One particularly important observation was made in 2014 independently by Chen *et al.* [10] as well as Kübler and Felser [11], who theoretically showed that noncollinear antiferromagnets can exhibit an anomalous Hall effect (AHE), a phenomenon traditionally ascribed to magnets with a (weak) ferromagnetic moment [12–14]. Their prediction was experimentally verified soon afterward [15,16]. It turned out that the existence of an AHE comes down to the question of whether the magnetic point group of the crystal is compatible with ferromagnetism [9,17–21]. Although such superordinate symmetry arguments were already brought forward by Kleiner in the 1960s [17–19], it took almost 50 years to rediscover this effect, which is explained in the modern language of Berry curvature [14,22–24].

Another research field, in which the charge degree of freedom and the associated Joule heating are abandoned and the transport of collective excitations of the magnetic order itself are studied, is that of spincaloritronics in insulators [25,26]. This field was recently topologically augmented with the prediction and the discovery of the magnon thermal Hall effect (ThHE; a transverse heat current response upon application of a longitudinal temperature gradient) [27–31] and the identification of magnon Chern insulators [32,33]. These magnon Chern phases protect chiral magnon edge states which may serve as highways for spin currents [32,34–38] and gave birth to the field of topological magnonics [37]. Moreover, the possibility of topologically nontrivial magnons in quantum magnets spawned broad fundamental interest and opened the quest for discovering more exotic objects like Weyl [39,40], Dirac [41–46], nodal-line [42,47], triple-point [48,49], and Floquet magnons [50].

Herein, we focus on the ThHE because it is routinely measured in experiments [28,51–55]. The present situation in the field of anomalous magnon heat currents is similar to that of anomalous electronic currents before publication of the seminal works of Chen *et al.* [10] as well as Kübler and Felser [11]. To the best of the authors' knowledge, all of the established materials (or models) that exhibit a magnon ThHE rely either on collinear ferromagnetism with Dzyaloshinskii-Moriya interaction (DMI), dipolar or related interactions [27–30,32,33,38,51,52,56–73], or on weak ferromagnetism with a nonzero scalar spin chirality, and/or an external magnetic field [49,53,74–87]; a ferromagnetic moment or an external magnetic field appear mandatory. In contrast, antiferromagnetism was studied (as far as transverse magnon transport is concerned) in the context of a transverse spin current response in collinear antiferromagnets, in which the transverse heat current response is rendered exactly zero by symmetry [88–94].

Given that rigorous symmetry analyses of linear transport tensors [20] (which were motivated in great part by electronic charge and spin transport but are independent of the microscopic degrees of freedom, i.e., independent of the carriers) allow for a ThHE in certain antiferromagnets, the above outlined situation clearly draws an incomplete picture of transverse magnon transport. This is the gap we wish to fill here by relying explicitly on the language of spin-wave theory and by presenting examples. We establish a connection between the fields of antiferromagnetism and that of topological magnons by predicting a magnon ThHE and a magnon Chern insulator in coplanar antiferromagnets. The two *necessary* demands on the antiferromagnet are (1) a broken effective time-reversal symmetry (TRS) and (2) a magnetic point group

compatible with ferromagnetism. This prediction not only vastly enlarges the class of magnetic crystals that exhibit topological magnons and transverse thermal magnon transport but also allows for a combination of anomalous magnon currents and the virtues of antiferromagnetism with respect to technical applications in magnon (spin)caloritronic devices.

We exemplify the prediction for a kagome antiferromagnet with the coplanar "inverse chiral order." Resemblant textures are found in metallic antiferromagnets like Mn_3Ge, Mn_3Ga, and Mn_3Sn [11] and in the mineral cadmium kapellasite $CdCu_3(OH)_6(NO_3)_2 \cdot H_2O$ [95]; we focus on the latter.

The paper is organized as follows. In Sec. II, we review linear spin-wave theory (LSWA), which is the framework within which we derive the two necessary conditions for a magnon ThHE. We then apply these results to kagome magnets and show that the coplanar inverse chiral order meets the requirements (Sec. III). This prediction is confirmed in Sec. IV, where we report on explicit calculations of the thermal Hall conductivity and Chern numbers within LSWA. In Sec. V, we comment on the approximate experimental realization of our model in cadmium kapellasite $CdCu_3(OH)_6(NO_3)_2 \cdot H_2O$ and estimate the thermal Hall signal. Finally, we conclude in Sec. VI.

II. SYMMETRY CONSIDERATIONS

The thermal Hall conductivity of a noninteracting Bose gas was derived in Refs. [29,30,57]:

$$\kappa_{\mu\nu} = -\frac{k_\mathrm{B}}{(2\pi)^3\hbar\beta}\sum_{n=1}^{N}\int_\mathrm{BZ} c_2[\rho(\varepsilon_{n\boldsymbol{k}},\beta)]\,\Omega_{n\boldsymbol{k}}^{\mu\nu}\,\mathrm{d}^3k. \tag{1}$$

Here, $\beta^{-1} = k_\mathrm{B}T$, k_B is Boltzmann's constant, T temperature, and $\hbar$ reduced Planck's constant. BZ denotes the first Brillouin zone and n is the band index. The weighting function [29,30,57]

$$c_2(x) = (1+x)\ln^2\tfrac{1+x}{x} - \ln^2 x - 2\,\mathrm{Li}_2(-x) \tag{2}$$

is evaluated for the bosonic distribution function $\rho(\varepsilon_{n\boldsymbol{k}},\beta) = [\exp(\beta\varepsilon_{n\boldsymbol{k}}) - 1]^{-1}$ with $\varepsilon_{n\boldsymbol{k}}$ denoting the magnon energies. Finally, $\Omega_{n\boldsymbol{k}}^{\mu\nu}$ is the magnon Berry curvature (its expression is given in Sec. II B) of the single-particle magnon Bloch wave functions. The aim of this section is to identify necessary requirements for a nonzero $\kappa_{\mu\nu}$ with $\mu \neq \nu$.

A. Brief reminder on linear spin-wave theory

To introduce notation, we review LSWA, using a formulation which is based in large part on the works of Haraldsen and Fishman [96], Petit [97], as well as Toth and Lake [98]. We mainly follow the notation of the latter.

Given a spin Hamiltonian of the form

$$H = \frac{1}{2}\sum_{i,j}\boldsymbol{S}_i^\mathrm{T} I_{ij}\boldsymbol{S}_j, \tag{3}$$

with spin operators $\boldsymbol{S}_i$ and $\boldsymbol{S}_j$ (at the lattice sites i and j, respectively), whose magnetic interactions are comprised in I_{ij}, one identifies the classical ground state by treating the quantum mechanical spins as classical vectors and minimizing the classical ground-state energy E_0. Once this is done, the number N of spins in the magnetic unit cell and their local directions $\hat{\boldsymbol{z}}_n$ $(n = 1,\ldots,N)$ are known. We rewrite the Hamiltonian as a sum over L magnetic unit cells (indexes i, j) and a sum over N magnetic basis sites (indexes n, m):

$$H = \frac{1}{2}\sum_{i,j}^{L}\sum_{m,n}^{N}\boldsymbol{S}_{m,i}^\mathrm{T} I_{ij}^{m,n}\boldsymbol{S}_{n,j}. \tag{4}$$

The local coordinate system $(\hat{\boldsymbol{x}}_n, \hat{\boldsymbol{y}}_n, \hat{\boldsymbol{z}}_n)$ of each spin has to be rotated onto the global coordinate system $(\hat{\boldsymbol{x}}, \hat{\boldsymbol{y}}, \hat{\boldsymbol{z}})$ to perform a local Holstein-Primakoff transformation [99]. With the associated local rotation matrix,

$$R_n = (\hat{\boldsymbol{x}}_n, \hat{\boldsymbol{y}}_n, \hat{\boldsymbol{z}}_n), \tag{5}$$

the transformation reads $\boldsymbol{S}_{n,j} = R_n\bar{\boldsymbol{S}}_{n,j}$ for the nth spin operator in the jth unit cell. Restricting ourselves to the harmonic excitation spectrum (noninteracting magnons), we perform a truncated Holstein-Primakoff transformation [99]:

$$\bar{\boldsymbol{S}}_{n,j} \approx \begin{pmatrix} \sqrt{S_n/2}(a_{j,n} + a_{j,n}^\dagger) \\ -\mathrm{i}\sqrt{S_n/2}(a_{j,n} - a_{j,n}^\dagger) \\ S_n - a_{j,n}^\dagger a_{j,n} \end{pmatrix}, \tag{6}$$

with $a_{j,n}^\dagger$ $(a_{j,n})$ being a bosonic creation (annihilation) operator. Within the global reference frame, we obtain [97,98]

$$\boldsymbol{S}_{j,n} \approx \sqrt{\frac{S_n}{2}}(\hat{\boldsymbol{u}}_n a_{j,n}^\dagger + \hat{\boldsymbol{u}}_n^* a_{j,n}) + \hat{\boldsymbol{z}}_n(S_n - a_{j,n}^\dagger a_{j,n}), \tag{7}$$

with $\hat{\boldsymbol{u}}_n \equiv \hat{\boldsymbol{x}}_n + \mathrm{i}\hat{\boldsymbol{y}}_n$. After a Fourier transformation,

$$a_{j,n}^{(\dagger)} = \frac{1}{\sqrt{L}}\sum_{\boldsymbol{k}} \mathrm{e}^{(-)\mathrm{i}(\boldsymbol{r}_j + \boldsymbol{t}_n)\cdot\boldsymbol{k}} a_{\boldsymbol{k},n}^{(\dagger)}, \tag{8}$$

where $\boldsymbol{r}_j$ is the position of the jth basis and $\boldsymbol{t}_n$ the vector to the nth spin in the basis, the bilinear Hamiltonian reads

$$H_2 = \frac{1}{2}\sum_{\boldsymbol{k}}\boldsymbol{\Psi}_{\boldsymbol{k}}^\dagger\mathcal{H}_{\boldsymbol{k}}\boldsymbol{\Psi}_{\boldsymbol{k}}, \tag{9}$$

with the linear spin-wave matrix

$$\mathcal{H}_{\boldsymbol{k}} = \begin{pmatrix} \mathcal{A}_{\boldsymbol{k}} - \mathcal{C} & \mathcal{B}_{\boldsymbol{k}} \\ \mathcal{B}_{\boldsymbol{k}}^\dagger & \mathcal{A}_{-\boldsymbol{k}}^\mathrm{T} - \mathcal{C} \end{pmatrix} \tag{10}$$

and the vector boson operator

$$\boldsymbol{\Psi}_{\boldsymbol{k}}^\dagger = (a_{\boldsymbol{k},1}^\dagger, \ldots, a_{\boldsymbol{k},N}^\dagger, a_{-\boldsymbol{k},1}, \ldots, a_{-\boldsymbol{k},N}). \tag{11}$$

The elements of the submatrices of the Hamilton matrix read [97,98]

$$(\mathcal{A}_{\boldsymbol{k}})_{m,n} = \frac{\sqrt{S_m S_n}}{2}\hat{\boldsymbol{u}}_m^\mathrm{T}\mathcal{I}_{\boldsymbol{k}}^{mn}\hat{\boldsymbol{u}}_n^*, \tag{12a}$$

$$(\mathcal{B}_{\boldsymbol{k}})_{m,n} = \frac{\sqrt{S_m S_n}}{2}\hat{\boldsymbol{u}}_m^\mathrm{T}\mathcal{I}_{\boldsymbol{k}}^{mn}\hat{\boldsymbol{u}}_n, \tag{12b}$$

$$(\mathcal{C})_{m,n} = \delta_{m,n}\sum_l S_l\hat{\boldsymbol{z}}_m^\mathrm{T}\mathcal{I}_{\boldsymbol{0}}^{ml}\hat{\boldsymbol{z}}_l, \tag{12c}$$

which include the Fourier transformed interaction matrix:

$$\mathcal{I}_{\boldsymbol{k}}^{mn} = \sum_i I^{mn}(\boldsymbol{\delta}_i)\,\mathrm{e}^{\mathrm{i}\boldsymbol{k}\cdot\boldsymbol{\delta}_i}. \tag{13}$$

The $\boldsymbol{\delta}_i$ are the difference vectors between the mth and the nth spin and $I^{mn}(\boldsymbol{\delta}_i)$ is the interaction matrix for this pair of spins.

To find the magnetic normal modes $b_{n\boldsymbol{k}}$ with energies $\varepsilon_{n\boldsymbol{k}}$, a paraunitary Bogoliubov transformation [100]

$$\mathcal{E}_{\boldsymbol{k}} \equiv T_{\boldsymbol{k}}^{\dagger}\mathcal{H}_{\boldsymbol{k}}T_{\boldsymbol{k}} = \mathrm{diag}(\varepsilon_{1,\boldsymbol{k}},\ldots,\varepsilon_{N,\boldsymbol{k}},\varepsilon_{1,-\boldsymbol{k}},\ldots,\varepsilon_{N,-\boldsymbol{k}}) \tag{14}$$

is performed, which diagonalizes

$$H_2 = \sum_{\boldsymbol{k}}\sum_{n=1}^{N}\varepsilon_{n\boldsymbol{k}}\left(b_{n\boldsymbol{k}}^{\dagger}b_{n\boldsymbol{k}} + \frac{1}{2}\right). \tag{15}$$

The paraunitarity, which is mathematically expressed as [100]

$$T_{\boldsymbol{k}}^{\dagger}GT_{\boldsymbol{k}} = G, \tag{16a}$$

$$G = \mathrm{diag}(\underbrace{1,\ldots,1}_{N},\underbrace{-1,\ldots,-1}_{N}), \tag{16b}$$

arises from the need of a canonical transformation, leaving the bosonic commutation rules intact.

B. Condition (1): Broken effective time-reversal symmetry

For a coplanar spin texture in the plane normal to a direction $\hat{\boldsymbol{e}}$, a combination of actual time reversal $\mathcal{T}$ (reversal of all spins $\mathcal{T}: \boldsymbol{S}_i \to -\boldsymbol{S}_i$; i site index) and a spin rotation by π about $\hat{\boldsymbol{e}}$ maps the texture onto itself. This is called an effective TRS $\mathcal{T}'$ [10,21,101]. Let us address its implications within LSWA.

We re-express the local coordinate system associated with the nth spin of the magnetic basis in terms of the local rotation matrix as

$$R_n = (\hat{\boldsymbol{e}}\times\hat{\boldsymbol{z}}_n, \hat{\boldsymbol{e}}, \hat{\boldsymbol{z}}_n). \tag{17}$$

Defining $\hat{\boldsymbol{u}}_n \equiv \hat{\boldsymbol{e}}\times\hat{\boldsymbol{z}}_n + \mathrm{i}\hat{\boldsymbol{e}}$, we obtain the same expression as in Eq. (7). An inversion of time flips all spin components, and, thus, all axes of this coordinate system, i.e., $R_i \to -R_i$. We then have to rotate the local coordinate systems to align $-\hat{\boldsymbol{z}}_n$ with the old spin direction $\hat{\boldsymbol{z}}_n$. Performing this rotation by π about $\hat{\boldsymbol{e}}$, we get

$$R_n' \equiv (\hat{\boldsymbol{e}}\times\hat{\boldsymbol{z}}_n, -\hat{\boldsymbol{e}}, \hat{\boldsymbol{z}}_n). \tag{18}$$

Thus, $\hat{\boldsymbol{u}}_n' \equiv \hat{\boldsymbol{e}}\times\hat{\boldsymbol{z}}_n - \mathrm{i}\hat{\boldsymbol{e}} = \hat{\boldsymbol{u}}_n^*$ and the new Holstein-Primakoff transformed spins read

$$\boldsymbol{S}_{j,n}' \approx \sqrt{\frac{S_n}{2}}(\hat{\boldsymbol{u}}_n^* a_{j,n}^{\dagger} + \hat{\boldsymbol{u}}_n a_{j,n}) + \hat{\boldsymbol{z}}_n(S_n - a_{j,n}^{\dagger}a_{j,n}). \tag{19}$$

Taking Eqs. (12a)–(12c) into account, the new LSWA Hamilton matrix reads

$$\mathcal{H}_{\boldsymbol{k}}' = \begin{pmatrix} \mathcal{A}_{-\boldsymbol{k}}^* - C & \mathcal{B}_{-\boldsymbol{k}}^* \\ \mathcal{B}_{-\boldsymbol{k}}^{\mathrm{T}} & \mathcal{A}_{\boldsymbol{k}}^{\dagger} - C \end{pmatrix} = \mathcal{H}_{-\boldsymbol{k}}^*. \tag{20}$$

Thus, if effective TRS $\mathcal{T}'$ is a symmetry of the magnet, i.e., if $\mathcal{H}_{\boldsymbol{k}}' = \mathcal{H}_{\boldsymbol{k}}$, we have

$$\mathcal{H}_{-\boldsymbol{k}} = \mathcal{H}_{\boldsymbol{k}}^* = \mathcal{T}'\mathcal{H}_{\boldsymbol{k}}(\mathcal{T}')^{-1}, \tag{21}$$

with $\mathcal{T}' = \mathcal{K}$ being the complex conjugation operation. Since $(\mathcal{T}')^2 = +1$, this is just the usual spinless (or bosonic) TRS.

We now show the implications of $\mathcal{T}'$ symmetry for the magnon Berry curvature. First, we can use Eq. (21) in the eigenvalue equation

$$\mathcal{H}_{\boldsymbol{k}}T_{\boldsymbol{k}} = GT_{\boldsymbol{k}}G\mathcal{E}_{\boldsymbol{k}} \tag{22}$$

to find

$$\mathcal{H}_{-\boldsymbol{k}}T_{\boldsymbol{k}}^* = GT_{\boldsymbol{k}}^*G\mathcal{E}_{\boldsymbol{k}}. \tag{23}$$

Thus, for every eigenvector matrix $T_{\boldsymbol{k}}$ of $\mathcal{H}_{\boldsymbol{k}}$ with eigenvalue matrix $G\mathcal{E}_{\boldsymbol{k}}$ there is a time-reversed partner eigenvector matrix $T_{\boldsymbol{k}}^*$ of $\mathcal{H}_{-\boldsymbol{k}}$ with the same eigenvalues; this implies

$$\mathcal{E}_{\boldsymbol{k}} = \mathcal{E}_{-\boldsymbol{k}}. \tag{24}$$

With this result and replacing $\boldsymbol{k} \to -\boldsymbol{k}$, Eq. (23) yields

$$\mathcal{H}_{\boldsymbol{k}}T_{-\boldsymbol{k}}^* = GT_{-\boldsymbol{k}}^*G\mathcal{E}_{\boldsymbol{k}}. \tag{25}$$

Comparing with Eq. (22), we see that $T_{\boldsymbol{k}}$ and $T_{-\boldsymbol{k}}^*$ obey the same eigenvalue equation, implying that they differ only by a phase factor matrix, i.e., a diagonal matrix with phase factor entries [57]. These phase factors can be ignored when studying the Berry curvature [57],

$$\Omega_{n\boldsymbol{k}}^{\mu\nu} = -2\mathrm{Im}\sum_{m\neq n}^{2N}\frac{(GT_{\boldsymbol{k}}^{\dagger}\partial_{\mu}\mathcal{H}_{\boldsymbol{k}}T_{\boldsymbol{k}})_{nm}(GT_{\boldsymbol{k}}^{\dagger}\partial_{\nu}\mathcal{H}_{\boldsymbol{k}}T_{\boldsymbol{k}})_{mn}}{[(G\mathcal{E}_{\boldsymbol{k}})_{nn} - (G\mathcal{E}_{\boldsymbol{k}})_{mm}]^2}, \tag{26}$$

since it is gauge-invariant. Taking the complex conjugate of the summands flips its sign, because of taking the imaginary part. Using Eq. (21), $(T_{\boldsymbol{k}}^{\dagger})^* = T_{-\boldsymbol{k}}^{\dagger}$, and $T_{\boldsymbol{k}}^* = T_{-\boldsymbol{k}}$ we find

$$\Omega_{n\boldsymbol{k}}^{\mu\nu} = -\Omega_{n,-\boldsymbol{k}}^{\mu\nu}. \tag{27}$$

Thus, if $\mathcal{T}'$ is a symmetry of the magnet, the magnon Berry curvature of the single-magnon Bloch wave functions is an odd function with respect to quasimomentum $\boldsymbol{k}$. Putting an odd $\Omega_{n\boldsymbol{k}}^{\mu\nu}$ into Eq. (1) and combining this with the $\boldsymbol{k}$-even energies [cf. Eq. (24)], renders the thermal Hall response zero. In converse, this means that a broken $\mathcal{T}'$ symmetry is a necessary requirement for a ThHE.

C. Condition (2): Magnetic point group compatible with ferromagnetism

Breaking the effective TRS does not imply that the thermal Hall conductivity is nonzero. Magneto-spatial symmetries $\mathcal{X}$ that belong to the magnetic point group of the crystal may still render the transverse heat current response zero, if $\Omega_{n,\boldsymbol{k}}^{\mu\nu} = -\Omega_{n,\mathcal{X}\boldsymbol{k}}^{\mu\nu}$.

Necessary conditions for the AHE of electrons have been studied in the past [17–21]. Those arguments can be carried over one-to-one to the magnonic case. In essence, the magnetization vector and the (transverse) heat conductivity vector,

$$\boldsymbol{M}^{\mathrm{T}} = (M_x, M_y, M_z), \tag{28}$$

$$\boldsymbol{\kappa}^{\mathrm{T}} = (\kappa_{yz}, \kappa_{zx}, \kappa_{xy}), \tag{29}$$

transform similarly under magnetic point group symmetry operations [21]. Thus, only if an element of $\boldsymbol{M}$ is compatible with the magnetic point group, the respective element of $\boldsymbol{\kappa}$ is also compatible. A list of all symmetry elements that forbid

certain components of the electronic anomalous conductivity was given in Ref. [21]. More broadly, symmetry-restricted linear transport tensor shapes were determined in Ref. [20], which apply to any microscopic carrier.

III. APPLICATION TO KAGOME MAGNETS

We have seen in the previous section that both a broken effective TRS and a magnetic point group compatible with ferromagnetism are necessary for a nonzero ThHE. The latter does not imply the actual presence of a ferromagnetic component. Antiferromagnets with sufficiently low symmetry may belong to such a magnetic point group, as is known from the recent studies of the electronic AHE [7,9–11,15,16,21]. To make a prediction of an *antiferromagnetic magnon ThHE* explicit, we particularize the discussion for magnetic textures on a kagome lattice. The analysis is based on the spin Hamiltonian

$$H = -\frac{J}{2}\sum_{\langle ij\rangle} \boldsymbol{S}_i \cdot \boldsymbol{S}_j + \frac{1}{2}\sum_{\langle ij\rangle} \boldsymbol{D}_{ij} \cdot \boldsymbol{S}_i \times \boldsymbol{S}_j \qquad (30)$$

($\langle ij\rangle$ indicates nearest neighbor summation) with isotropic Heisenberg exchange J and Dzyaloshinskii-Moriya vector $\boldsymbol{D}_{ij}$ [102], which—according to Moriya's rules [103]—is perpendicular to the bond direction. While out-of-plane components of $\boldsymbol{D}_{ij}$ are always allowed by symmetry, the existence of nonzero in-plane components requires that the kagome plane, which is thought to be part of a three-dimensional crystal, is not a mirror plane [104]. In the following, we write $\boldsymbol{D}_{ij} = \nu_{ij}\,(D_\parallel\,\hat{n}^x_{ij}, D_\parallel\,\hat{n}^y_{ij}, D_z)$, where D_z and $D_\parallel$ are the strengths of out-of-plane and in-plane DMI, respectively. $\hat{\boldsymbol{n}}_{ij}$ is the direction of the in-plane DMI (orthogonal to the bonds, pointing towards or away from a triangle's center of gravity) and $\nu_{ij} = \pm 1$, depending on the orientation of the bond ij. The signs of the DMI components follow the convention of Ref. [104].

In the following, we recall two well-known mechanisms of breaking effective TRS. First, ferromagnetism with DMI (collinear kagome ferromagnets) [27,33,52,56,59,66,105,106] and, second, weak ferromagnetism with nonzero spin chirality (noncoplanar kagome antiferromagnets) [77,84]. Then we turn to coplanar antiferromagnets.

A. Collinear kagome ferromagnet

A ferromagnet is obtained for $J > 0$ and the magnetization points, for example, in $+z$ direction. Considering the case of mirror symmetry ($D_\parallel = 0$), the DMI energy $D_z\,(S^x_i S^y_j - S^y_i S^x_j)$ is not invariant under rotation by π about any in-plane axis. If $D_z \neq 0$, $\mathcal{T}'$ symmetry is broken and condition (1) is met. Since this system belongs to the magnetic point group $6/mm'm'$, a ThHE is expected. This scenario is at least approximately realized in Cu(1,3-benzenedicarboxylate) [106–108], for which a ThHE was measured [52].

B. Noncoplanar kagome antiferromagnet

According to Ref. [104], a weak ferromagnet with positive vector spin chirality (all-in–all-out order) is obtained for antiferromagnetic exchange $J < 0$ (which by itself prefers any 120° coplanar order), positive $D_z > 0$ (which favors the ground state with positive over the one with negative vector chirality), and $D_\parallel$ that leads to the out-of-plane canting of the ground state (nonzero scalar spin chirality, i.e., nonzero solid angles). For noncoplanar spins, it is impossible to find a common axis to rotate the time-reversed spins back onto the original ones [21] and, hence, $\mathcal{T}'$ symmetry is broken. The magnetic point group $\bar{3}1m'$ allows for a ThHE.

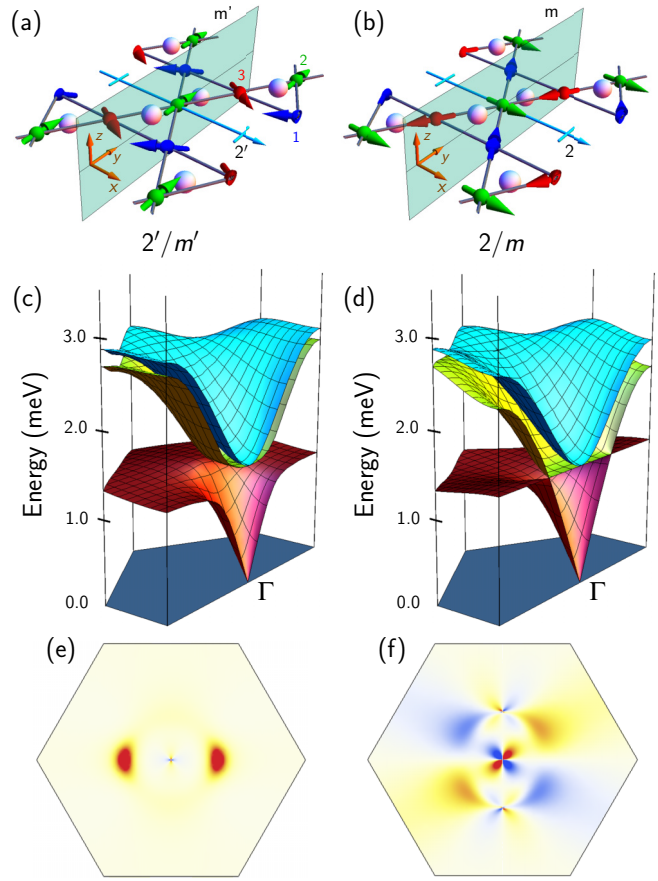

FIG. 1. Magnetic texture with negative vector chirality on the kagome lattice. Top row: Magnetic ground states with the three spins of the magnetic unit cell shown in blue, green and red, respectively. Symmetry operations of the respective magnetic point groups $2'/m'$ (a) and $2/m$ (b) are indicated, with a prime marking additional time reversal. White spheres refer to entities that break the mirror symmetry of the kagome plane. Second row: Spin-wave dispersions of the system sketched in (a) and (b). Only one half of the first Brillouin zone with center Γ is shown. Third row: Berry curvature $\Omega^{xy}_{1,\boldsymbol{k}}$ of the lowest band of (c) and (d) (red: positive; white: zero; blue: negative). Parameters read $S = 1$, $J = 5D_z = -2D_\parallel = -1$ meV.

C. Coplanar inverse chiral kagome antiferromagnet

The coplanar antiferromagnetic order with negative vector spin chirality shown in Figs. 1(a) and 1(b) is central to the present investigation. This classical ground state is stable for antiferromagnetic exchange $J < 0$, $D_z < 0$, and $D_\parallel$ with modulus less than a certain critical value [104]. In contrast to the positive chiral order, the coplanar inverse chiral order is robust for nonzero $D_\parallel$ (no out-of-plane canting) because it

favors the opposite vector chirality [104]. The inverse chiral order belongs to an infinitely degenerate manifold of classical ground states [two of which are shown in Figs. 1(a) and 1(b)] obtained by a rigid in-plane rotation of all spins.

The details of the ground state are essential to the study of thermal transport. Assuming a single magnetic domain, the magnetic point group of texture (a) is $2'/m'$ while that of (b) is $2/m$. Both are compatible with ferromagnetism but differ in their ferromagnetic component: that of $2'/m'$ (a) is within the mirror plane and that of $2/m$ (b) points along the twofold rotation axis. This translates into transport tensors with different shapes (cf. Tables V and VI of Ref. [20]; notice the difference in the choice of coordinates):

$$\kappa_{2'/m'} = \begin{pmatrix} \kappa_{xx} & \kappa_{xy} & -\kappa_{xz} \\ -\kappa_{xy} & \kappa_{yy} & \kappa_{yz} \\ \kappa_{xz} & \kappa_{yz} & \kappa_{zz} \end{pmatrix}, \tag{31a}$$

$$\kappa_{2/m} = \begin{pmatrix} \kappa_{xx} & 0 & 0 \\ 0 & \kappa_{yy} & \kappa_{yz} \\ 0 & \kappa_{zy} & \kappa_{zz} \end{pmatrix}. \tag{31b}$$

In particular, only the order depicted in Fig. 1(a) allows for a ThHE within the kagome plane ($\kappa_{xy} \neq 0$). Thus, these two representatives of the classically degenerate ground-state manifold behave fundamentally different in macroscopic transport experiments. An analysis of zero-point fluctuations is therefore in order (see Sec. IV).

With magnetic point groups compatible with ferromagnetism, these antiferromagnets exhibit a ThHE, if $\mathcal{T}'$ symmetry is broken. The mapping of the time-reversed spins back onto the original coplanar order is achieved only by a π rotation about the z axis. It transforms the spins as $\mathcal{R}^z_\pi(S^x_i, S^y_i, S^z_i) \to (-S^x_i, -S^y_i, S^z_i)$, which leaves $D_z\,(S^x_i S^y_j - S^y_i S^x_j)$ invariant. Only products that connect in-plane (S^x_i, S^y_i) with out-of-plane spin components (S^z_i) break $\mathcal{T}'$. However, such terms vanish if the kagome plane is a mirror plane [109]. Conversely, only breaking this mirror symmetry, i.e., for $D_\parallel \neq 0$, breaks $\mathcal{T}'$ as well because both $S^y_i S^z_j - S^z_i S^y_j$ and $S^z_i S^x_j - S^x_i S^z_j$ change sign and are thus not invariant under $\mathcal{R}^z_\pi$. Note that we have assumed broken mirror plane symmetry for the determination of the magnetic point groups [white spheres in Figs. 1(a) and 1(b) refer to mirror-symmetry-breaking entities].

In sum, the above symmetry arguments show that *coplanar* kagome antiferromagnets with inverse chiral texture meet the necessary conditions for a magnon ThHE.

IV. LINEAR SPIN-WAVE ANALYSIS OF INVERSE CHIRAL KAGOME ANTIFERROMAGNETS

We now explicitly calculate the transport properties within LSWA. For parametrizing the classically degenerate ground-state manifold, we define the global rotation angle α as the angle of the green spin in Fig. 1(a) with the y direction [$\alpha = 0$ in Fig. 1(a), $\alpha = -\pi/2$ in Fig. 1(b)]. Following Sec. II, the linear spin-wave matrix of the inverse chiral order becomes

$$\mathcal{H}_{\boldsymbol{k}} = \frac{S}{2}\begin{pmatrix} \mathcal{A}_{\boldsymbol{k}} - \mathcal{C} & \mathcal{B}_{\boldsymbol{k}} \\ \mathcal{B}^\dagger_{\boldsymbol{k}} & \mathcal{A}^{\mathrm{T}}_{-\boldsymbol{k}} - \mathcal{C} \end{pmatrix}, \tag{32}$$

with $\mathcal{C} = 4 j_+ \mathcal{I}_{3\times 3}$ and

$$\mathcal{A}_{\boldsymbol{k}} = \begin{pmatrix} 0 & [j_- - \mathrm{i}D_\parallel(\cos\alpha + \sqrt{3}\sin\alpha)]c_{12} & [j_- - 2\mathrm{i}D_\parallel\cos\alpha]c_{13} \\ [j_- + \mathrm{i}D_\parallel(\cos\alpha + \sqrt{3}\sin\alpha)]c_{12} & 0 & [j_- - \mathrm{i}D_\parallel(\cos\alpha - \sqrt{3}\sin\alpha)]c_{23} \\ [j_- + 2\mathrm{i}D_\parallel\cos\alpha]c_{13} & [j_- + \mathrm{i}D_\parallel(\cos\alpha - \sqrt{3}\sin\alpha)]c_{23} & 0 \end{pmatrix}, \tag{33a}$$

$$\mathcal{B}_{\boldsymbol{k}} = \begin{pmatrix} 0 & [j'_+ + \mathrm{i}D_\parallel(3\cos\alpha - \sqrt{3}\sin\alpha)]c_{12} & [j'_+ + 2\sqrt{3}\mathrm{i}D_\parallel\sin\alpha]c_{13} \\ [j'_+ + \mathrm{i}D_\parallel(3\cos\alpha - \sqrt{3}\sin\alpha)]c_{12} & 0 & [j'_+ - \mathrm{i}D_\parallel(3\cos\alpha + \sqrt{3}\sin\alpha)]c_{23} \\ [j'_+ + 2\sqrt{3}\mathrm{i}D_\parallel\sin\alpha]c_{13} & [j'_+ - \mathrm{i}D_\parallel(3\cos\alpha + \sqrt{3}\sin\alpha)]c_{23} & 0 \end{pmatrix}\mathrm{e}^{2\mathrm{i}\alpha}, \tag{33b}$$

in which

$$j_\pm \equiv \sqrt{3}D_z \pm J, \tag{34a}$$

$$j'_+ \equiv \sqrt{3}D_z + 3J, \tag{34b}$$

$$c_{\mu\nu} \equiv \cos(\boldsymbol{k}\cdot\boldsymbol{\delta}_{\mu\nu}), \tag{34c}$$

and

$$\boldsymbol{\delta}^{\mathrm{T}}_{12} = (-1, \sqrt{3})/2, \tag{35a}$$

$$\boldsymbol{\delta}^{\mathrm{T}}_{13} = (-1, 0), \tag{35b}$$

$$\boldsymbol{\delta}^{\mathrm{T}}_{23} = (-1, -\sqrt{3})/2. \tag{35c}$$

The factor of $\mathrm{e}^{2\mathrm{i}\alpha}$ in Eq. (33b) can always be absorbed into the bosonic vectors by a transformation $\tilde{\boldsymbol{\Psi}}_{\boldsymbol{k}} = \mathcal{P}^{-1}(\alpha)\boldsymbol{\Psi}_{\boldsymbol{k}}$, where

$$\mathcal{P}(\alpha) = \mathrm{diag}(\mathrm{e}^{\mathrm{i}\alpha}, \mathrm{e}^{\mathrm{i}\alpha}, \mathrm{e}^{\mathrm{i}\alpha}, \mathrm{e}^{-\mathrm{i}\alpha}, \mathrm{e}^{-\mathrm{i}\alpha}, \mathrm{e}^{-\mathrm{i}\alpha}). \tag{36}$$

Then, the Hamilton matrix reads

$$\tilde{\mathcal{H}}_{\boldsymbol{k}} = \mathcal{P}^{-1}(\alpha)\mathcal{H}_{\boldsymbol{k}}\mathcal{P}(\alpha) = \frac{S}{2}\begin{pmatrix} \mathcal{A}_{\boldsymbol{k}} - \mathcal{C} & \mathcal{B}_{\boldsymbol{k}}\mathrm{e}^{-2\mathrm{i}\alpha} \\ \mathcal{B}^\dagger_{\boldsymbol{k}}\mathrm{e}^{2\mathrm{i}\alpha} & \mathcal{A}^{\mathrm{T}}_{-\boldsymbol{k}} - \mathcal{C} \end{pmatrix}. \tag{37}$$

For $D_\parallel = 0$, the relation $\tilde{\mathcal{H}}_{-\boldsymbol{k}} = \tilde{\mathcal{H}}^*_{\boldsymbol{k}}$ holds, indicating effective TRS and the absence of ThHEs as explained in Sec. II B. This symmetry is broken for nonzero $D_\parallel$. This finding is in agreement with the qualitative arguments in Sec. III.

We now diagonalize $\tilde{\mathcal{H}}_{\boldsymbol{k}}$ as explained in Sec. II. The bilinear Hamiltonian becomes

$$H_2 = \sum_{\boldsymbol{k}} \sum_{n=1}^{3} \varepsilon_{n\boldsymbol{k}}(\alpha)\left(b_{n\boldsymbol{k}}^{\dagger} b_{n\boldsymbol{k}} + \frac{1}{2}\right), \tag{38}$$

where $\varepsilon_{n\boldsymbol{k}}(\alpha)$ are the angle-dependent magnon energies. The zero-point fluctuations correct the classical ground-state energy and depend on the rotation angle α. The corrected ground-state energy is minimal for $\alpha = p \cdot \pi/3$ (p integer), indicating that quantum fluctuations prefer the texture in Fig. 1(a) over that in Fig. 1(b). However, magnetocrystalline anisotropies may select Fig. 1(b) over Fig. 1(a), as is the case in cadmium kapellasite $CdCu_3(OH)_6(NO_3)_2 \cdot H_2O$ due to a local $\langle 100 \rangle$ easy-axis anisotropy [95]. Thus, both textures are relevant for experiment and worth studying.

The linear spin-wave dispersion relation for $\alpha = 0$ exhibits the twofold rotational symmetry of the magnetic point group [Fig. 1(c)]. There is a band gap between the lowest and the other bands. The out-of-plane Berry curvature $\Omega_{1,\boldsymbol{k}}^{xy}$ of the lowest band [Fig. 1(e)] is predominantly positive, indicating a nonzero thermal Hall integral. Thus, $\kappa_{xy} \neq 0$ in agreement with the above symmetry arguments and Eq. (31a).

The Chern number

$$C_n = \frac{1}{2\pi} \int_{\mathrm{BZ}} \Omega_{n,\boldsymbol{k}}^{xy} \, \mathrm{d}^2 k \tag{39}$$

reads

$$C_1 = (-1)^p \operatorname{sgn} D_{\parallel} \tag{40}$$

for the lowest band. Thus, the coplanar inverse chiral spin texture of Fig. 1(a) realizes an *antiferromagnetic* magnonic Chern insulator (or topological magnon insulator [33]). According to the bulk-boundary correspondence [110,111], nonzero Chern numbers imply the existence of chiral magnon edge states. The Chern numbers depend on the sign of $D_{\parallel}$ and the rotation angle $\alpha = p \cdot \pi/3$. A multidomain antiferromagnet built from both p-even and p-odd domains hosts topologically protected unidirectionally propagating magnons at the domain walls [112].

With respect to ThHE measurements, single domain magnets are preferable because the thermal Hall signals of domains with opposite Chern numbers cancel. A small in-plane magnetic field could be utilized to prefer energetically the magnetic order associated with one particular p. Rotating this field (and, hence, varying α) manifests itself in oscillations of $\kappa_{xy}^{\mathrm{3D}}$ [113] (Fig. 2). The alternating sign is due to the alternating relative orientation of the spins with respect to the in-plane DM vectors. For the magnetic excitations, opposite spin orders (one spin pointing towards or away from the center of gravity of a triangle, as sketched in Fig. 2) effectively reverse $D_{\parallel}$, which explains the sign reversal of the Chern numbers and of κ_{xy}.

The linear spin-wave dispersions for $\alpha = -\pi/2$ exhibit no band gap but two touching points [Fig. 1(d)]. The Berry curvature has positive as well as negative contributions, so that its Brillouin zone integral vanishes and $\kappa_{xy} = 0$, in agreement with the above reasoning and Eq. (31b). This result is expected for any spin texture with $\alpha = -\pi/2 + p \cdot \pi/3$. Any of these spin configurations can be understood as an intermediate of two configurations with $\alpha = p \cdot \pi/3$ and $\alpha = (p \pm 1) \cdot \pi/3$, respectively, which have nonzero but opposite κ_{xy} (insets in Fig. 2).

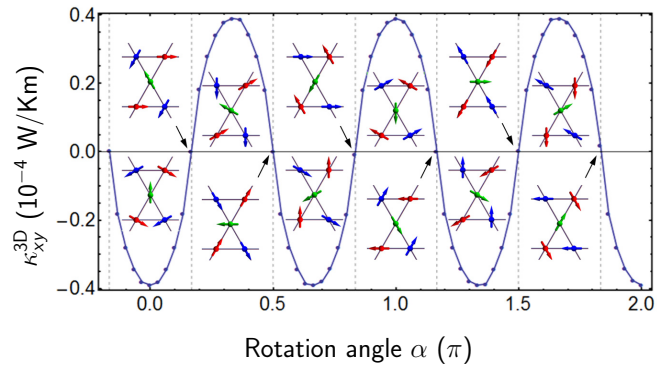

FIG. 2. In-plane thermal Hall conductivity $\kappa_{xy}^{\mathrm{3D}}$ versus the spin rotation angle α. Insets show the spin texture for $\alpha = m \cdot \pi/6$ with integer m. Parameters as in Fig. 1, $T = 3\,K$.

V. REALIZATION IN CADMIUM KAPELLASITE

As recently reported by Okuma *et al.* [95], the inverse chiral texture due to DMI is found in single-crystalline cadmium kapellasite $CdCu_3(OH)_6(NO_3)_2 \cdot H_2O$. This material is an $S = 1/2$ antiferromagnet with an ordering temperature of $T_{\mathrm{N}} \sim 4\,\mathrm{K}$. A weak ferromagnetic moment in the plane is due to local $\langle 100 \rangle$ easy-axis anisotropy (almost $\alpha = -\pi/2$; the angle between any two spins deviates slightly from 120°). If in a single-domain state, its thermal transport tensor should therefore have the form of $\kappa_{2/m}$ in Eq. (31b); in particular, $\kappa_{xy} = 0$.

The magnetic parameters were estimated as $J = 3.88\,\mathrm{meV}$ and $D = \sqrt{D_z^2 + D_{\parallel}^2} \sim 0.1\,J$ [95]. The observation that a weak $\langle 100 \rangle$ anisotropy [95] "wins out" over $D_{\parallel}$, as far as the selection of the ground-state texture is concerned, does not necessarily imply a small $D_{\parallel}$ because the zero-point fluctuations have small amplitude. In the following, we assume that the anisotropy is so small that it is easily overcome by a small in-plane magnetic field that stabilizes the $\alpha = p \cdot \pi/3$ order [e.g., $\alpha = 0$ in Fig. 1(a)]. We may then approximately describe cadmium kapellasite by the spin Hamiltonian in Eq. (30), noting that anisotropies and a magnetic field lead to minor distortions of the magnon dispersion. Doing so, the magnitude of κ_{xy} is heavily influenced by the angle θ of $\boldsymbol{D}$ with the kagome plane (that is the ratio $D_{\parallel}/D_z$). For example, increasing θ from $-\pi/4$ to $-\pi/12$ (increasing in-plane component) leads to an increase (in absolute value) of the thermal Hall conductivity from $\kappa_{xy}^{\mathrm{3D}} \sim -10^{-6}\,\mathrm{W/K/m}$ to $-10^{-5}\,\mathrm{W/K/m}$ at $T = 3\,\mathrm{K}$, which is just within experimentally accessible range [52]. Thus, the ThHE probes effectively the directions of the DM vectors.

VI. CONCLUSION

We predicted a magnon ThHE in coplanar antiferromagnets and introduced a model for an *antiferromagnetic*

magnonic Chern phase. Our findings are in line with the rigorous symmetry analysis of (spin) transport tensors of Ref. [20] and the recent work on the electronic AHE in noncollinear antiferromagnets [7,9–11,15,16,21]. We demonstrated explicitly that neither an external field, nor a ferromagnetic net moment, nor a scalar spin chirality are necessary for a magnon ThHE. As an approximate material realization, we proposed cadmium kapellasite $CdCu_3(OH)_6(NO_3)_2 \cdot H_2O$.

ACKNOWLEDGMENT

This work is supported by SPP 1666 of Deutsche Forschungsgemeinschaft (DFG).

[1] V. Baltz, A. Manchon, M. Tsoi, T. Moriyama, T. Ono, and Y. Tserkovnyak, Rev. Mod. Phys. **90**, 015005 (2018).

[2] T. Jungwirth, J. Sinova, A. Manchon, X. Marti, J. Wunderlich, and C. Felser, Nat. Phys. **14**, 200 (2018).

[3] R. Duine, K.-J. Lee, S. S. Parkin, and M. D. Stiles, Nat. Phys. **14**, 217 (2018).

[4] O. Gomonay, V. Baltz, A. Brataas, and Y. Tserkovnyak, Nat. Phys. **14**, 213 (2018).

[5] J. Železný, P. Wadley, K. Olejník, A. Hoffmann, and H. Ohno, Nat. Phys. **14**, 220 (2018).

[6] P. Němec, M. Fiebig, T. Kampfrath, and A. V. Kimel, Nat. Phys. **14**, 229 (2018).

[7] L. Šmejkal, Y. Mokrousov, B. Yan, and A. H. MacDonald, Nat. Phys. **14**, 242 (2018).

[8] M. B. Jungfleisch, W. Zhang, and A. Hoffmann, Phys. Lett. A **382**, 865 (2018).

[9] L. Šmejkal and T. Jungwirth, in *Topology in Magnetism*, edited by J. Zang, V. Cros, and A. Hoffmann (Springer International Publishing, Cham, 2018), Chap. 9.

[10] H. Chen, Q. Niu, and A. H. MacDonald, Phys. Rev. Lett. **112**, 017205 (2014).

[11] J. Kübler and C. Felser, Europhys. Lett. **108**, 67001 (2014).

[12] E. Hall, Philos. Mag Series 5 **12**, 157 (1881).

[13] Y. Taguchi, Y. Oohara, H. Yoshizawa, N. Nagaosa, and Y. Tokura, Science **291**, 2573 (2001).

[14] N. Nagaosa, J. Sinova, S. Onoda, A. H. MacDonald, and N. P. Ong, Rev. Mod. Phys. **82**, 1539 (2010).

[15] S. Nakatsuji, N. Kiyohara, and T. Higo, Nature **527**, 212 (2015).

[16] A. K. Nayak, J. E. Fischer, Y. Sun, B. Yan, J. Karel, A. C. Komarek, C. Shekhar, N. Kumar, W. Schnelle, J. Kübler *et al.*, Sci. Adv. **2**, e1501870 (2016).

[17] W. H. Kleiner, Phys. Rev. **142**, 318 (1966).

[18] W. H. Kleiner, Phys. Rev. **153**, 726 (1967).

[19] W. H. Kleiner, Phys. Rev. **182**, 705 (1969).

[20] M. Seemann, D. Ködderitzsch, S. Wimmer, and H. Ebert, Phys. Rev. B **92**, 155138 (2015).

[21] M.-T. Suzuki, T. Koretsune, M. Ochi, and R. Arita, Phys. Rev. B **95**, 094406 (2017).

[22] M. V. Berry, Proc. R. Soc. London A **392**, 45 (1984).

[23] J. Zak, Phys. Rev. Lett. **62**, 2747 (1989).

[24] G. Sundaram and Q. Niu, Phys. Rev. B **59**, 14915 (1999).

[25] K. Uchida, J. Xiao, H. Adachi, J.-i. Ohe, S. Takahashi, J. Ieda, T. Ota, Y. Kajiwara, H. Umezawa, H. Kawai *et al.*, Nat. Mater. **9**, 894 (2010).

[26] G. E. Bauer, E. Saitoh, and B. J. Van Wees, Nat. Mater. **11**, 391 (2012).

[27] H. Katsura, N. Nagaosa, and P. A. Lee, Phys. Rev. Lett. **104**, 066403 (2010).

[28] Y. Onose, T. Ideue, H. Katsura, Y. Shiomi, N. Nagaosa, and Y. Tokura, Science **329**, 297 (2010).

[29] R. Matsumoto and S. Murakami, Phys. Rev. Lett. **106**, 197202 (2011).

[30] R. Matsumoto and S. Murakami, Phys. Rev. B **84**, 184406 (2011).

[31] Note that prior to the ThHE a transverse spin current response due to magnetic-field gradients was theoretically predicted [114], [115].

[32] R. Shindou, R. Matsumoto, S. Murakami, and J.-I. Ohe, Phys. Rev. B **87**, 174427 (2013).

[33] L. Zhang, J. Ren, J.-S. Wang, and B. Li, Phys. Rev. B **87**, 144101 (2013).

[34] M. Pereiro, D. Yudin, J. Chico, C. Etz, O. Eriksson, and A. Bergman, Nat. Commun. **5**, 4815 (2014).

[35] A. Mook, J. Henk, and I. Mertig, Phys. Rev. B **91**, 174409 (2015).

[36] X. S. Wang, Y. Su, and X. R. Wang, Phys. Rev. B **95**, 014435 (2017).

[37] X. S. Wang, H. W. Zhang, and X. R. Wang, Phys. Rev. Appl. **9**, 024029 (2018).

[38] A. Rückriegel, A. Brataas, and R. A. Duine, Phys. Rev. B **97**, 081106 (2018).

[39] F.-Y. Li, Y.-D. Li, Y. B. Kim, L. Balents, Y. Yu, and G. Chen, Nat. Commun. **7**, 12691 (2016).

[40] A. Mook, J. Henk, and I. Mertig, Phys. Rev. Lett. **117**, 157204 (2016).

[41] J. Fransson, A. M. Black-Schaffer, and A. V. Balatsky, Phys. Rev. B **94**, 075401 (2016).

[42] K. Li, C. Li, J. Hu, Y. Li, and C. Fang, Phys. Rev. Lett. **119**, 247202 (2017).

[43] N. Okuma, Phys. Rev. Lett. **119**, 107205 (2017).

[44] S. Owerre, Sci. Rep. **7**, 6931 (2017).

[45] S. S. Pershoguba, S. Banerjee, J. C. Lashley, J. Park, H. Ågren, G. Aeppli, and A. V. Balatsky, Phys. Rev. X **8**, 011010 (2018).

[46] W. Yao, C. Li, L. Wang, S. Xue, Y. Dan, K. Iida, K. Kamazawa, K. Li, C. Fang, and Y. Li, Nat. Phys. **14**, 1011 (2018).

[47] A. Mook, J. Henk, and I. Mertig, Phys. Rev. B **95**, 014418 (2017).

[48] S. Owerre, Europhys. Lett. **120**, 57002 (2018).

[49] K. Hwang, N. Trivedi, and M. Randeria, arXiv:1712.08170.

[50] S. Owerre, J. Phys. Commun. **1**, 021002 (2017).

[51] T. Ideue, Y. Onose, H. Katsura, Y. Shiomi, S. Ishiwata, N. Nagaosa, and Y. Tokura, Phys. Rev. B **85**, 134411 (2012).

[52] M. Hirschberger, R. Chisnell, Y. S. Lee, and N. P. Ong, Phys. Rev. Lett. **115**, 106603 (2015).

[53] M. Hirschberger, J. W. Krizan, R. J. Cava, and N. P. Ong, Science **348**, 106 (2015).

[54] T. Ideue, T. Kurumaji, S. Ishiwata, and Y. Tokura, Nat. Mater. **16**, 797 (2017).

[55] H. Doki, M. Akazawa, H.-Y. Lee, J. H. Han, K. Sugii, M. Shimozawa, N. Kawashima, M. Oda, H. Yoshida, and M. Yamashita, Phys. Rev. Lett. **121**, 097203 (2018).

[56] A. Mook, J. Henk, and I. Mertig, Phys. Rev. B **89**, 134409 (2014).

[57] R. Matsumoto, R. Shindou, and S. Murakami, Phys. Rev. B **89**, 054420 (2014).

[58] X. Cao, K. Chen, and D. He, J. Phys.: Condens. Matter **27**, 166003 (2015).

[59] H. Lee, J. H. Han, and P. A. Lee, Phys. Rev. B **91**, 125413 (2015).

[60] B. Xu, T. Ohtsuki, and R. Shindou, Phys. Rev. B **94**, 220403 (2016).

[61] K. Nakata, J. Klinovaja, and D. Loss, Phys. Rev. B **95**, 125429 (2017).

[62] S. A. Owerre, J. Phys.: Condens. Matter **28**, 386001 (2016).

[63] S. A. Owerre, J. Appl. Phys. **120**, 043903 (2016).

[64] S. A. Owerre, Phys. Rev. B **94**, 094405 (2016).

[65] S. A. Owerre, J. Phys.: Condens. Matter **28**, 47LT02 (2016).

[66] A. Mook, J. Henk, and I. Mertig, Phys. Rev. B **94**, 174444 (2016).

[67] B. Madon, D. C. Pham, J.-E. Wegrowe, D. Lacour, M. Hehn, V. Polewczyk, A. Anane, and V. Cros, Phys. Rev. B **94**, 144423 (2016).

[68] A. Okamoto and S. Murakami, Phys. Rev. B **96**, 174437 (2017).

[69] S. Murakami and A. Okamoto, J. Phys. Soc. Jpn. **86**, 011010 (2017).

[70] S. A. Owerre, J. Phys.: Condens. Matter **29**, 185801 (2017).

[71] B. Li and A. A. Kovalev, Phys. Rev. B **97**, 174413 (2018).

[72] R. Seshadri and D. Sen, Phys. Rev. B **97**, 134411 (2018).

[73] M. Kawano and C. Hotta, arXiv:1805.05872.

[74] K. A. van Hoogdalem, Y. Tserkovnyak, and D. Loss, Phys. Rev. B **87**, 024402 (2013).

[75] C. Schütte and M. Garst, Phys. Rev. B **90**, 094423 (2014).

[76] A. Mook, B. Göbel, J. Henk, and I. Mertig, Phys. Rev. B **95**, 020401 (2017).

[77] S. A. Owerre, Phys. Rev. B **95**, 014422 (2017).

[78] S. A. Owerre, J. Phys.: Condens. Matter **29**, 03LT01 (2017).

[79] S. A. Owerre, Europhys. Lett. **117**, 37006 (2017).

[80] S. A. Owerre, J. Appl. Phys. **121**, 223904 (2017).

[81] E. Iacocca and O. Heinonen, Phys. Rev. Appl. **8**, 034015 (2017).

[82] P. Laurell and G. A. Fiete, Phys. Rev. Lett. **118**, 177201 (2017).

[83] S. A. Owerre, Canadian J. Phys. **96**, 1216 (2018).

[84] P. Laurell and G. A. Fiete, Phys. Rev. B **98**, 094419 (2018).

[85] J. Cookmeyer and J. E. Moore, Phys. Rev. B **98**, 060412 (2018).

[86] S. K. Kim, K. Nakata, D. Loss, and Y. Tserkovnyak, arXiv:1808.06690.

[87] We also note the related Hall effects of Schwinger bosons [55,59,116], triplons [117,118], and magnetoelastic excitations [54,119].

[88] R. Cheng, S. Okamoto, and D. Xiao, Phys. Rev. Lett. **117**, 217202 (2016).

[89] V. A. Zyuzin and A. A. Kovalev, Phys. Rev. Lett. **117**, 217203 (2016).

[90] K. Nakata, S. K. Kim, J. Klinovaja, and D. Loss, Phys. Rev. B **96**, 224414 (2017).

[91] Y. Shiomi, R. Takashima, and E. Saitoh, Phys. Rev. B **96**, 134425 (2017).

[92] A. Mook, B. Göbel, J. Henk, and I. Mertig, Phys. Rev. B **97**, 140401 (2018).

[93] K. H. Lee, S. B. Chung, K. Park, and J.-G. Park, Phys. Rev. B **97**, 180401 (2018).

[94] A notable exception is Ref. [115], in which a transverse spin current due to a gradient in a magnetic field was predicted in a coplanar magnet, a setup we are not going to investigate.

[95] R. Okuma, T. Yajima, D. Nishio-Hamane, T. Okubo, and Z. Hiroi, Phys. Rev. B **95**, 094427 (2017).

[96] J. Haraldsen and R. Fishman, J. Phys.: Condens. Matter **21**, 216001 (2009).

[97] S. Petit, JDN **12**, 105 (2011).

[98] S. Toth and B. Lake, J. Phys.: Condens. Matter **27**, 166002 (2015).

[99] T. Holstein and H. Primakoff, Phys. Rev. **58**, 1098 (1940).

[100] J. Colpa, Phys. A: Stat. Mech. App. **93**, 327 (1978).

[101] P. Bruno, *Magnetism Goes Nano: Electron Correlations, Spin Transport, Molecular Magnetism; Lecture Manuscripts of the 36th Spring School of the Institute of Solid State Research*, edited by S. Blügel, T. Brückel, and C. M. Schneider, Schriften des Forschungszentrums Jülich. Reihe Materie und Material/Matter and Material (Forschungszentrum, Zentralbibliothek, Jülich, 2005), Vol. 26, Chap. 9.

[102] I. Dzyaloshinsky, J. Phys. Chem. Sol. **4**, 241 (1958).

[103] T. Moriya, Phys. Rev. **120**, 91 (1960).

[104] M. Elhajal, B. Canals, and C. Lacroix, Phys. Rev. B **66**, 014422 (2002).

[105] A. Mook, J. Henk, and I. Mertig, Phys. Rev. B **90**, 024412 (2014).

[106] R. Chisnell, J. S. Helton, D. E. Freedman, D. K. Singh, R. I. Bewley, D. G. Nocera, and Y. S. Lee, Phys. Rev. Lett. **115**, 147201 (2015).

[107] E. A. Nytko, J. S. Helton, P. Müller, and D. G. Nocera, J. Am. Chem. Soc. **130**, 2922 (2008).

[108] R. Chisnell, J. S. Helton, D. E. Freedman, D. K. Singh, F. Demmel, C. Stock, D. G. Nocera, and Y. S. Lee, Phys. Rev. B **93**, 214403 (2016).

[109] K. Essafi, O. Benton, and L. D. C. Jaubert, Phys. Rev. B **96**, 205126 (2017).

[110] Y. Hatsugai, Phys. Rev. B **48**, 11851 (1993).

[111] Y. Hatsugai, Phys. Rev. Lett. **71**, 3697 (1993).

[112] A. Mook, J. Henk, and I. Mertig, Phys. Rev. B **91**, 224411 (2015).

[113] We define $\kappa_{xy}^{\mathrm{3D}} \equiv \kappa_{xy}/d$, where $d = 0.7\,nm$ is a realistic spacing of kagome layers [95]. Each of the layers shows a thermal Hall conductivity κ_{xy} obtained from Eq. (1) in the two-dimensional limit $(2\pi)^3 \to (2\pi)^2$ and $\mathrm{d}^3k \to \mathrm{d}^2k$.

[114] F. Meier and D. Loss, Phys. Rev. Lett. **90**, 167204 (2003).

[115] S. Fujimoto, Phys. Rev. Lett. **103**, 047203 (2009).

[116] S. K. Kim, H. Ochoa, R. Zarzuela, and Y. Tserkovnyak, Phys. Rev. Lett. **117**, 227201 (2016).

[117] J. Romhányi, K. Penc, and R. Ganesh, Nat. Commun. **6**, 6805 (2015).

[118] M. Malki and K. P. Schmidt, Phys. Rev. B **95**, 195137 (2017).

[119] R. Takahashi and N. Nagaosa, Phys. Rev. Lett. **117**, 217205 (2016).